Published in Biochemistry 45, issue 27, pp. 8243–8253, 2006,
which should be used for any reference to this work

Probing the Active Site of *Pseudomonas aeruginosa* Porphobilinogen Synthase Using Newly Developed Inhibitors[†]

Frederic Frère,[‡,§] Merle Nentwich,[‡] Sabine Gacond,[||] Dirk W. Heinz,[⊥] Reinhard Neier,[||] and Nicole Frankenberg-Dinkel*[,‡,@]

Institute for Microbiology, Technical University Braunschweig, Spielmannstrasse 7, D-38106 Braunschweig, Germany
Institute of Chemistry, University of Neuchâtel, Avenue de Bellevaux 51, Case postale 2, CH-2007 Neuchâtel, Switzerland
Department of Structural Biology, German Research Center for Biotechnology, Mascheroder Weg 1, D-38124 Braunschweig, Germany

ABSTRACT: Porphobilinogen synthase catalyzes the first committed step of the tetrapyrrole biosynthesis pathway. In an aldol-like condensation, two molecules of 5-aminolevulinic acid (ALA) form the first pyrrole, porphobilinogen. Newly synthesized analogues of a reaction intermediate of porphobilinogen synthase have been employed in studying the active site and the catalytic mechanism of this early enzyme of tetrapyrrole biosynthesis. This study combines structural and kinetic evaluation of the inhibition potency of these inhibitors. In addition, one of the determined protein structures provides for the first time structural evidence of a magnesium ion in the active site. From these results, we can corroborate an earlier postulated enzymatic mechanism that starts with formation of a C−C bond, linking C3 of the A-side ALA to C4 of the P-side ALA through an aldole addition. The obtained data are discussed with respect to the current literature.

Porphobilinogen synthase (PBGS,[1] EC 4.2.1.24), also called 5-aminolevulinic acid dehydratase (ALAD), catalyzes the first common step during the biosynthesis of tetrapyrroles such as hemes, chlorophylls, and bilins (*1*, *2*). During the catalytic process, the asymmetric condensation of two molecules of 5-aminolevulinic acid (ALA) yields the first pyrrole porphobilinogen (PBG) (Figure 1). PBGSs from a wide variety of organisms have been studied in detail, and crystal structures of many have been published (*3*−*7*). The most common active form of PBGS is a homo-octamer, but it has been shown that lower oligomeric states can be catalytically active as well (*8*). Each monomer consists of a classical eight-stranded $(\beta\alpha)_8$ barrel with the active site located at the C-terminal ends of the β-strands. A flexible loop (lid) covers the active site and separates it from the surrounding medium. The two ALA substrate molecules are distinguished as A- and P-side ALA due to the acetic acid and propanoic acid side chains, respectively, that they contribute to the product PBG. The corresponding binding sites of PBGS are termed the A-site and P-site, respectively.

Although it is a family of highly homologous enzymes, significant variation can be observed in the employment of metal ions at catalytic and allosteric sites. The PBGS from *Pseudomonas aeruginosa* (*Pa*PBGS) contains four magnesium ions per octamer which are located at an allosteric site remote from the active site. Furthermore, monovalent cations have been found in the active site and also at the subunit interfaces (*9*, *10*). PBGSs from other organisms have been shown to contain zinc ions in the active site. Because of the variable requirement for metal ions, a phylogenetic diversity in the chemical reaction mechanism has been postulated depending on whether the enzyme carries an active site zinc ion (*11*). Despite the differences in metal ion utilization in the enzyme family, it is commonly accepted that the PBGS reaction starts with the binding of the P-side ALA. The subsequent step in the reaction is the binding of the second substrate molecule to the A-site. In zinc-dependent PBGS, the active site metal ion is essential for the binding of A-side ALA (*12*). Crystal structures support this scenario (*13*) (PDB entry 1e51).

On the basis of structural and biochemical data, we and others previously postulated a catalytic mechanism for PBGS

[†] This work was supported by grants from the Deutsche Forschungsgemeinschaft and the Fonds der chemischen Industrie to D.W.H. and N.F.-D., as well as a grant from the Swiss National Science Foundation (Grant 2000-104007) to R.N. N.F.-D. is a fellow of the Emmy-Noether-Program of the Deutsche Forschungsgemeinschaft.

* To whom correspondence should be addressed. Phone: +49 234 3223101. Fax: +49 234 3214620. E-mail: nicole.frankenberg@rub.de.
[‡] Technical University Braunschweig.
[§] Present address: Institute for Pharmacology und Toxicology, University of Zürich, Winterthurerstr. 190, CH-8057 Zürich, Switzerland.
[||] University of Neuchâtel.
[⊥] German Research Center for Biotechnology.
[@] Present address: Physiology of Microorganisms, Ruhr-University-Bochum, Universitätsstr. 150, D-44780 Bochum, Germany.

[1] Abbreviations: 5F-LA, 5-fluorolevulinic acid; LA, levulinic acid; 5-OH-LA, 5-hydroxylevulinic acid; ALA, 5-aminolevulinic acid; ALAD, aminolevulinic acid dehydratase; “amine”, 5-(4-carboxy-2-oxobutylamino)-4-oxopentanoic acid; *Ec*PBGS, porphobilinogen synthase from *E. coli*; “ether”, 5-(4-carboxy-2-oxobutoxy)-4-oxopentanoic acid; *Hs*PBGS, porphobilinogen synthase from *Homo sapiens*; *Pa*PBGS, porphobilinogen synthase from *P. aeruginosa*; PDB, Protein Data Bank; PBG, porphobilinogen; PBGS, porphobilinogen synthase; *Sc*PBGS, porphobilinogen synthase from *Saccharomyces cerevisiae*; “sulfone”, 5-(4-carboxy-2-oxobutane-1-sulfonyl)-4-oxopentanoic acid; “sulfoxide”, 5-(4-carboxy-2-oxobutane-1-sulfinyl)-4-oxopentanoic acid; “thioether”, 5-(4-carboxy-2-oxobutylsulfanyl)-4-oxopentanoic acid.

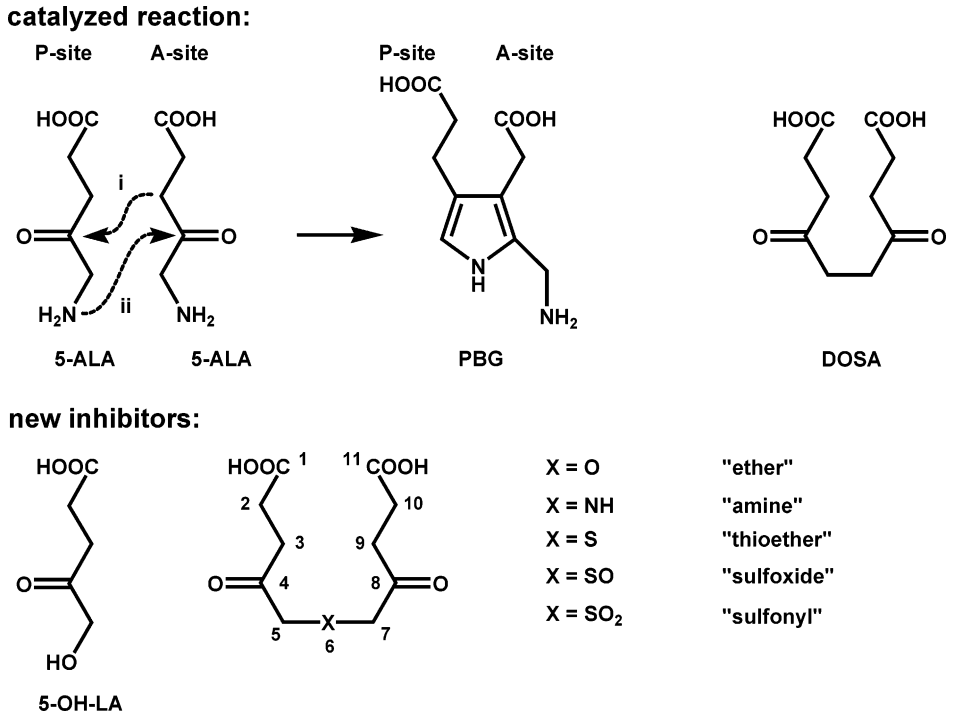

FIGURE 1: Reaction catalyzed by PBGS and inhibitors. Only trivial names are given.

initiated by the formation of Schiff bases between the two substrate molecules and two conserved lysine residues in the active site (*9*, *14*, *15*). Several studies suggest that the reaction proceeds with the formation of a C−C bond between C3 of the A-side ALA and C4 of the P-side ALA (*9*, *11*, *13*).

Despite the impressive efforts in studying PBGS and its multistep mechanism (*11*), many questions are still open. No unequivocal picture for the succession of the chemical transformations involved in the enzyme-catalyzed mechanism has emerged.

In this study, we have employed six synthesized inhibitors to probe the active site of *Pa*PBGS using X-ray crystallography. Five of the inhibitors resemble bisubstrate analogues (symmetric dicarboxy, di-γ-keto compounds) with variation of the central linking moiety. The sixth inhibitor is a close structural analogue of the substrate ALA (see Figure 1 for structures).

EXPERIMENTAL PROCEDURES

Construction of Expression Vector pLM_PBGS. The vector was constructed and kindly provided by L. Stith and E. K. Jaffe (Fox Chase Cancer Center, Philadelphia, PA). After insertion (*Nde*I) and internal removal (*BamH*I) of restriction sites via QuikChange mutagenesis, the *P. aeruginosa hemB* gene was excised from pGEX*hemB* (*16*) using *Nde*I and *Bam*HI and ligated into similarly digested pET3a, generating pLM_PBGS. The integrity of the plasmid construct was verified by DNA sequencing.

Protein Production and Purification. Freshly transformed *Escherichia coli* BL21(λDE3) cells containing vector pLM_PBGS were grown in 500 mL batches of LB medium containing 100 mg/L ampicillin and supplemented with 0.4% glucose. An inoculum from a single bacterial colony was grown at 37 °C and vigorously shaken for 16 h. The cells were harvested by centrifugation, resuspended in fresh LB medium, and cooled to 17 °C, and protein production was induced by adding IPTG to a final concentration of 100 μM. The cells were further grown at 17 °C overnight and subsequently harvested by centrifugation.

The bacterial pellet from a total growth of 1 L was resuspended in lysis buffer [50 mM Tris-HCl (pH 8.0), 100 mM NaCl, 0.05% Triton X-100, and 5 mM $MgCl_2$] containing a protease inhibitor cocktail (Roche Diagnostics) and disrupted with a French press ($2 \times 20\,000$ lb/in.^{2}). Cell debris was removed by centrifugation for 45 min at 100000*g*. The resulting supernatant was subjected to a 25% $(NH_4)_2SO_4$ precipitation at 4 °C overnight. After centrifugation at 4 °C for 20 min at 5000*g*, the pellet was resuspended in 50 mM HEPES-KOH (pH 8.0) and 5 mM $MgCl_2$ (buffer A) and directly loaded onto a phenyl-Sepharose column ($V = 10$ mL) which had been previously equilibrated with 50 mM HEPES-KOH (pH 8.0), 5 mM $MgCl_2$, and 20% $(NH_4)_2SO_4$ (buffer B). Unbound protein was removed by washing the column with 3 column volumes of buffer B. Protein was eluted with a linear gradient from 20 to 0% $(NH_4)_2SO_4$ in buffer A. PBGS-containing fractions were identified UV spectroscopically and by SDS−PAGE, pooled, and directly loaded onto a DEAE-Sepharose column ($V = 25$ mL) which had been equilibrated with buffer A. Protein was eluted with a linear gradient from 0 to 1 M KCl in buffer A. PBGS eluted with ∼500 mM KCl from the DEAE column. For further analysis, the enzyme was dialyzed against 100 mM Tris-HCl (pH 7.5) and 10 mM $MgCl_2$ and concentrated using Amicon concentrator devices (MWCO = 10 000). The yield of purified *P. aeruginosa* was approximately 100 mg from 1 L of bacterial culture.

Enzyme Activity Assay. The activity of PBGS was determined using a modified Ehrlich's test which is based on the reaction between the product PBG and 4-(dimethylamino)-benzaldehyde as described previously (*16*).

Determination of IC_{50} Values. IC_{50} values were determined to approximate the potency of the inhibitors. The assay

Table 1: Crystallization and Cryo Data

	5-OH-LA/*Pa*PBGS	"amine"/*Pa*PBGS	"ether"/*Pa*PBGS	"sulfoxide"/*Pa*PBGS	"sulfone"/*Pa*PBGS	"thioether"/*Pa*PBGS
protein solution	10 mg/mL protein, 50 mM Tris-HCl (pH 7.5), 5 mM $MgCl_2$, 10 mM 5-OH-LA sodium salt	10 mg/mL protein, 50 mM Tris-HCl (pH 7.5), 5 mM $MgCl_2$, 1 mM NaCl, 1 mM "amine" monosodium salt	10 mg/mL protein, 100 mM Tris-HCl (pH 7.5), 5 mM $MgCl_2$, 5 mM "ether"	10 mg/mL protein, 50 mM Tris-HCl (pH 7.5), 5 mM $MgCl_2$, 10 mM "sulfoxide" disodium salt	10 mg/mL protein, 50 mM Tris-HCl (pH 7.5), 5 mM $MgCl_2$, 10 mM "sulfone" disodium salt	10 mg/mL protein, 50 mM Tris-HCl (pH 7.5), 5 mM $MgCl_2$, 10 mM "thioether" disodium salt
reservoir	9.0% (w/v) PEG-4000, 180 mM KCl, 9 mM $CaCl_2$, 0.05 mM sodium cacodylate (pH 6.0),	18.0% (w/v) PEG-3350, 200 mM $LiNO_3$	12.0% (w/v) PEG-8000, 340 mM Li_2SO_4, 20% (v/v) glycerol	18.0% (w/v) PEG-3350, 220 mM LiCl	31.0% (v/v) PEG-400, 100 mM Na-HEPES (pH 7.5), 180 mM $MgCl_2$	17.0% (w/v) PEG-3350, 120 mM sodium tartrate
cryoprotective solution	20% (v/v) PEG-400, 80% reservoir solution	20% (v/v) PEG-400, 80% reservoir solution	crystal directly frozen in its mother liquor	20% (v/v) PEG-400, 80% reservoir solution	10% (v/v) PEG-400, 90% reservoir solution	20% (v/v) PEG-400, 80% reservoir solution

contained a final PBGS concentration of 4 μg/mL and varying final concentrations of inhibitor [from 125 mM (or lower due to solubility problems) to 12.5 μM] in a bis-tris-propane (BTP) buffer [100 mM BTP (pH 8.5) and 10 mM $MgCl_2$]. Stock solutions of protein, buffer, inhibitor, and water were mixed and incubated at 37 °C for 30 min. To start the reaction, substrate was added to a final concentration of 2 mM in a final volume of 400 μL. The mixture was incubated for 15 min. The PBGS-catalyzed reaction was then stopped by adding the reaction mixture (350 μL) to the stop reagent (350 μL) (25% trichloroacetic acid). After centrifugation (3 min at 5000*g*), the supernatant (450 μL) was treated with Ehrlich's reagent (450 μL) [0.4 g of 4-(dimethylamino)-benzaldehyde in 10 mL of acetic acid and 10 mL of perchloric acid]. After 15 min at room temperature, the amount of product was determined by measuring the absorbance at 555 nm ($\epsilon = 60\,200\ M^{-1}\ cm^{-1}$).

For determination of IC_{50} values, the data of the dose−response plot were fitted to eq 1.

$$\frac{A}{A_0} = \frac{1}{1 + \left(\frac{[I]}{IC_{50}}\right)^h} \quad (1)$$

where *h* is a Hill coefficient and accounts for potential deviations from a simple noncooperative inhibition model (see Discussion for details) (*17*).

Crystallization and Structure Determination. Protein solutions containing inhibitors were generated by mixing aliquots of protein solution [20 mg/mL protein, 100 mM Tris-HCl, and 10 mM $MgCl_2$ (pH 7.5)] and inhibitor solution (see Table 1 for final concentrations). Crystallization lead conditions were identified using Crystal Screen, Crystal Screen 2, Low Ionic Strength Screen, Natrix, and Crystal Screen Cryo sparse matrix screens (Hampton Research, Aliso Viejo, CA) in 96-well sitting-drop CrystalClear strip racks (Douglas Instruments) with 100 μL of reservoir solution and drops of 3 μL of reservoir and 3 μL of protein solution. Thereby produced initial conditions as well as known crystallization conditions for wild-type *Pa*PBGS (*5*) were optimized by the hanging-drop, vapor-diffusion method with 500 μL of reservoir solution and drops of 5 μL of protein and 5 μL of reservoir solution in linbro plates (Hampton Research) (Table 1). Prior to X-ray data collection, crystals were washed in a cryoprotective solution for 5 s and flash-frozen in liquid N_2 (Table 1). Data collection was performed under cryogenic conditions using Cu Kα radiation and a Rigaku-MSC R-Axis IV^{++} image plate or synchrotron radiation (PSF, BESSY, Berlin, Germany; beamline BL1, $\lambda = 0.98010$ Å) using a MAR Research CCD detector (Table 2).

The structures of *Pa*PBGS in complex with the inhibitors were determined by difference Fourier synthesis, using the refined model of wild-type *Pa*PBGS (PDB entry 1b4k). This was followed by several rounds of refinement using REFMAC5 (*18*, *19*) and ARP/wARP (*20*) and manual model building using O (*21*). Na^+, K^+, Mg^{2+}, and Cl^- and ethylene glycol oligomers were incorporated to match the electron density, temperature factors, and coordination sphere (*22* and references cited therein). In obvious cases, two to three alternate amino acid conformations were modeled. The quality of the structure was checked using PROCHECK (*23*) and WhatIf (*24*).

Analysis of protein−inhibitor interactions was facilitated by the use of ligplot (*25*). Overlays have been created using lsqkab as a part of the CCP4 suite (*18*). The overlay of the PBGSs from different organisms (Figure 4A) was generated by searching for the best fit for the backbone atoms of the eight central β-strands of these proteins to the respective residues of wild-type *Pa*PBGS (PDB entry 1b4k). Figures 3 and 4 were generated using PyMOL (DeLano Scientific LLC, South San Francisco, CA).

Structural coordinates were deposited in the PDB (Table 2).

RESULTS

Expression and Purification of Recombinant P. aeruginosa PBGS. P. aeruginosa PBGS was produced and purified from a new expression system which is under the control of a T7 promoter. The advantage of this system over the previous one (GST fusion) (*16*) is the extremely high protein yield (∼100 mg of protein per liter of bacterial culture) and the lack of an affinity tag for purification. Therefore, the recombinant protein employed in this study most closely resembles the native enzyme. The obtained protein was purified to ∼98% homogeneity.

Inhibition Potency of the Employed Inhibitors. Five analogues of a bisubstrate were synthesized (*26*) and tested in the standard PBGS assay system. Common to all compounds are the two carboxylate groups and two keto functions. The only difference between the analogues is the variation of the central function and consequently the volume

Table 2: X-ray and Refinement Data

	5-OH-LA	"amine"	"ether"	"sulfoxide"	"sulfone"	"thioether"
structure determination						
space group	$P42_12$	$P42_12$	$P42_12$	$P42_12$	$P42_12$	$P42_12$
cell dimensions						
a (Å)	126.31	126.88	127.54	125.51	125.60	127.20
b (Å)	126.31	126.88	127.54	125.51	125.60	127.20
c (Å)	85.48	86.10	85.79	86.77	86.57	85.85
total no. of reflections[a]	418190	433644	798378	297780	339607	467805
no. of unique reflections	37881	55853	117544	45985	55920	44731
resolution range (Å)[b]	40.2−2.15 (2.23−2.15)	40.13−1.90 (1.94−1.90)	38.10−1.48 (1.51−1.48)	39.68−2.02 (2.07−2.02)	39.50−1.93 (1.98−1.93)	34.26−2.05 (2.10−2.05)
completeness (%)[b]	99.2 (99.5)	98.8 (95.2)	96.2 (98.2)	99.8 (99.8)	95.0 (93.4)	97.8 (97.7)
redundancy[b]	11.0 (9.9)	7.8 (7.0)	6.8 (6.1)	6.5 (6.0)	6.1 (5.5)	10.5 (9.5)
R_{merge}[b,c]	12.6 (45.6)	16.3 (48.3)	8.0 (36.0)	4.1 (22.6)	11.6 (47.9)	12.3 (46.2)
I/σ_I[b]	16.7 (4.9)	9.9 (2.0)	19.3 (3.1)	38.0 (4.17)	11.7 (3.46)	14.5 (4.3)
temperature factor (Å^2)	22.5	19.2	10.6	17.9	20.3	20.9
refinement						
resolution range used for refinement (Å)[d]	89.8−2.15	89.8−1.90	90.17−1.48	89.8−2.02	89.8−1.93	89.8−2.05
no. of reflections[a]	35917	52367	107399	43556	47003	41499
no. of non-H protein atoms/dimer	6020	6349	6841	6395	6180	6273
no. of solvent molecules/dimer	456	723	968	654	639	659
no. of ions/dimer						
Na^+	−	−	−	−	2	2
K^+	2	−	−	−	−	−
Mg^{2+}	2	2	2	2	7	2
Cl^-	2	−	−	1	2	−
average *B*-factor (Å^2)	17.70	18.02	11.31	15.63	19.11	18.43
R-factor (%), R_{free} (%)[e]	15.5, 20.4	15.99, 20.12	14.91, 17.11	14.48, 18.33	15.13, 18.63	14.66, 20.11
Ramachandran plot[f] (%)						
most favored regions	92.6	94.6	94.1	93.4	93.0	93.5
additionally allowed regions	6.8	5.4	5.9	6.6	6.8	6.5
generously allowed regions	0.4	0.0	0.0	0.0	0.0	0.0
rms deviation from ideality						
bond lengths (Å)	0.017	0.016	0.008	0.015	0.015	0.016
bond angles (deg)[g]	1.696	1.525	1.249	1.474	1.469	1.497
estimated overall coordinate error, based on maximum likelihood (Å)	0.112	0.089	0.036	0.088	0.085	0.097
beamline	home source	Bessy, PSF, BL1	Bessy, PSF, BL1	Bessy, PSF, BL1	Bessy, PSF, BL1	home source
PDB entry	2c13	2c14	2c15	2c16	2c18	2c19

[a] Greater than 1σ. [b] Value for the highest-resolution shell in parentheses. [c] $R_{merge} = 100(\sum_{h,i}|I_{h,i}I_h|/\sum_{h,i} I_{h,i})$, where summation is over all $I_{h,i}$ observations contributing to the I_h reflection intensities. [d] F_c for a range of 87.71−20.0 Å. [e] Five percent of the data was omitted from refinement (*42*). [f] Calculated using Procheck (*23*). [g] Calculated using Whatif (*24*).

and polarity of this moiety (Figure 1). It has been shown previously that the carboxylate group and the γ-keto groups are essential for recognition by the enzyme (*27*, *28*). In addition to the bisubstrate analogues, one single-substrate analogue, 5-hydroxylevulinic acid (5-OH-LA), was employed (*29*).

To approximate the potency of the inhibitors, their IC_{50} values were determined using protein and substrate concentrations comparable to those used in earlier studies (*9*, *14*, *30*). The data are summarized in Figure 2, and deduced IC_{50} values are listed in Table 3. "Ether", "amine", and "thioether" are decent inhibitors with IC_{50} values of <1 mM, whereas the three others displayed weaker inhibition potency. Data obtained for "sulfone" and "sulfoxide" were the only ones that fit eq 1 with a Hill coefficient (*h*) that deviated significantly from unity (Table 3).

Crystal Structures of the Active Site of P. aeruginosa PBGS with the Various Inhibitors. Because of the excellent crystallization behavior of *Pa*PBGS, we were able to determine structures with each inhibitor bound. All enzymes display the same overall fold that has been described for the wild-type enzyme (*5*). The loop covering the active site ("active site flap") of monomer A is ordered in all structures except for "sulfoxide"/*Pa*PBGS, while in "sulfone"/*Pa*PBGS, it displays a hitherto unobserved but ordered conformation.

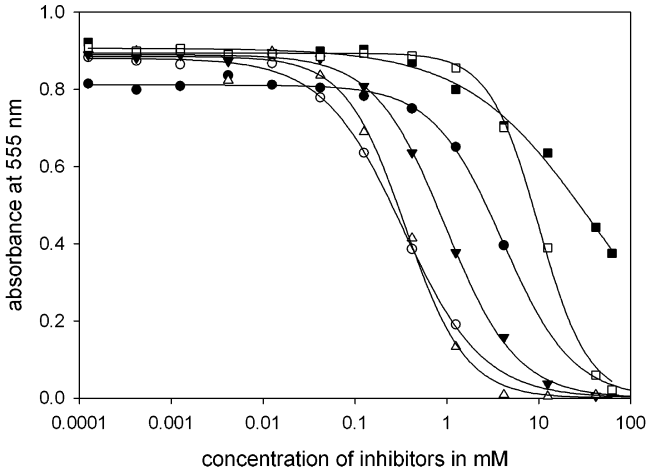

FIGURE 2: Dose−response plots for the determination of IC_{50} values. Shown is the dependence of product formation (here shown as absorbance at 555 nm for the complex of PBG with Ehrlich's reagent) on inhibitor concentration: (●) 5-OH-LA, (○) "amine", (▼) "ether", (△) "thioether", (■) "sulfoxide", and (□) "sulfone".

Table 3: IC_{50} Values for the Employed Inhibitors

inhibitor	IC_{50} (mM)	Hill coefficient (*h*)
5-OH-LA	4.05	∼1
"ether"	0.963	∼1
"amine"	0.313	∼1
"sulfoxide"	38.4	0.64
"sulfone"	9.94	1.61
"thioether"	0.342	∼1

In the case of "sulfone"/*Pa*PBGS, this might be due to the special binding of the inhibitor (see below) that induces slight changes (C_α atom shifts of D131 and Q138 of approximately 0.8 and 1.0 Å, respectively) in the loop connecting D131 to D139 lying adjacent to the active site flap. In "sulfoxide"/*Pa*PBGS, Q138 and H136 exhibit two alternative, shifted positions potentially contributing to a destabilization of the active site flap. All residues responsible for coordination of the inhibitors, including R215 and K229, are nevertheless well resolved in all structures.

The crystal structure of *Pa*PBGS in complex with 5-OH-LA is of certain interest, as this inhibitor is the closest possible structural and chemical mimic of ALA (Figure 1). Because of this, it is able to perform very similar interactions with the enzyme, although its is unable to undergo the condensation reaction. Two molecules of 5-OH-LA are bound to the A- and P-site. Both are fixed via Schiff bases to K205 and K260, and their conformation is analogous to the binding of 5F-LA (Figure 3A) (*9*). Nevertheless, the interactions of the moieties in the 5 position of inhibitor species 5F-LA and 5-OH-LA differ notably. While the two fluorine atoms of the 5F-LA molecules coordinate a monovalent cation that is integrated into a network of hydrophilic interactions, the hydroxy groups of the A-site 5-OH-LA inhibitor directly interact with the respective residues (D139 and S175) through H-bonds. Furthermore, the inhibitor in the P-site is stabilized not only through the Schiff base fixation to K260 but also via the fixation of the carboxylic group through interactions with Y324 and S286 and via hydrophobic interactions between the inhibitors' apolar part (C2−C5) and F86, Y202, Y211, F214, and Y283. The A-side 5-OH-LA is fixed via the Schiff base to K205 but also forms hydrophilic interactions with its carboxylic group with R215, K229, Q233, and a water molecule and with D139 and S175 (O and O_γ) with its hydroxyl group. On the basis of the similarity between 5-OH-LA and the substrate, we propose that the complex represents a snapshot of the onset of catalysis (Figure 5). Recently, the structure of yeast PBGS in complex with 5-OH-LA was determined. In contrast to the structure presented here, 5-OH-LA is bound in two conformations in the yeast PBGS but only to the P-site lysine residue (*31*).

The high-resolution structure of "ether"/*Pa*PBGS gives an ambiguous picture of the inhibitor's binding (Figure 3B): The P-side part of "ether" including the ether moiety as well as C2 and the carboxylic group of the A-side part are nicely defined by electron density, while the rest of the molecule (except partly the keto group) is flexible and not resolved in the electron density. This part was modeled with the most likely conformation based on conformational constraints. The second Schiff base in the A-site is not formed according to the electron density. The conformation of the defined part in the P-site is identical to the conformation found in 5F-LA/*Pa*PBGS (*9*), 5-OH-LA/*Pa*PBGS, and ALA/*Sc*PBGS (*32*) (Figure 4A,B) structures, allowing comparable interactions of both the carboxylic group (hydrophilic) and the apolar part (C7−C10, hydrophobic) with the surrounding residues. Furthermore, the interactions responsible for the recognition of the A-side carboxylic group and the positioning of this group are consistent with the 5-OH-LA/*Pa*PBGS structure. The C4 keto moiety possibly deploys H-bonds to two of the water molecules present in the active site.

The determination of the structures of *Pa*PBGS in complex with "amine" and "thioether" revealed additional insights (Figure 3C,D). Both inhibitors are covalently linked with their C4 and C8 atoms to the amino moieties of K205 and K260, respectively. Interestingly, in both cases, the structure reveals continuous electron density directly connecting C3 and C8 of the inhibitors, indicating that a C−C bond has been formed. We postulate that initially both keto moieties of the inhibitors have been linked to the lysines via Schiff bases followed by an aldole addition of C3 of the A-side to C8 of the P-side. Consequently, bond formation brings the two parts of the inhibitor and thereby the lysine amino groups closer together. Nevertheless, no significant rearrangements of the surrounding residues are observed when they are compared to the 5F-LA/*Pa*PBGS, 5-OH-LA/*Pa*PBGS, and ALA/*Sc*PBGS structures (Figure 4A). Instead, the P-side part of the inhibitor changes its conformation except the carboxylic group which is kept fixed in its position (Figure 3A,C,D). For the same reasons, the position of the A-side carboxylic group is slightly shifted in both structures. Thereby, these "upper" parts of the reacted inhibitors (comprising C1 to C4 and C8 to C11 in A- and P-side, respectively) serve as a model for an intermediate, in which the C−C bond formation has occurred. This can be seen in an overlay of these inhibitors with this respective intermediate that had been modeled in the structure of *Hs*PBGS mutant F12L (*7*) [intermediate 1, Figure 5/IV and Figure 4C]. This comparison underscores the relevance of these reacted inhibitors as mimics of reaction intermediates.

The reacted inhibitors are stabilized by hydrophobic interactions with M177, A204, Y211, F214, Y283, V285, and S286. As found for all bound compounds so far (Figure 4A−C), the P-side carboxylic groups of "amine" and "thioether" are fixed through H-bonds to S286 (O_γ and N) and Y324. Their A-side carboxylic groups interact with R215, K229, Q233, and a water molecule that is part of a hydrophilic network at the A-site, which also includes D131, D139, S175, and two additional water molecules. In contrast to the hydrophobic thioether moiety of "thioether", the secondary amino moiety of "amine" forms an additional H-bond with one of these two water molecules.

The structure of "sulfoxide"/*Pa*PBGS is much like those of "amine"/*Pa*PBGS and "thioether"/*Pa*PBGS except for the differences in the loop connecting D131 to D139 (Figure 3E). Again, formation of a C−C bond has occurred, and its conformation and interaction with the surrounding residues are analogous to those of "amine" and "thioether" except for the sulfoxide moiety. The amine moiety is a H-bond donor, while the thioether is apolar. The sulfoxide moiety on the contrary is bulkier and a H-bond acceptor. In this structure, the side chains of D131 and D139 are moved slightly away from the inhibitor compared to those of 5-OH-LA/*Pa*PBGS and *Pa*PBGS possibly due to this change in

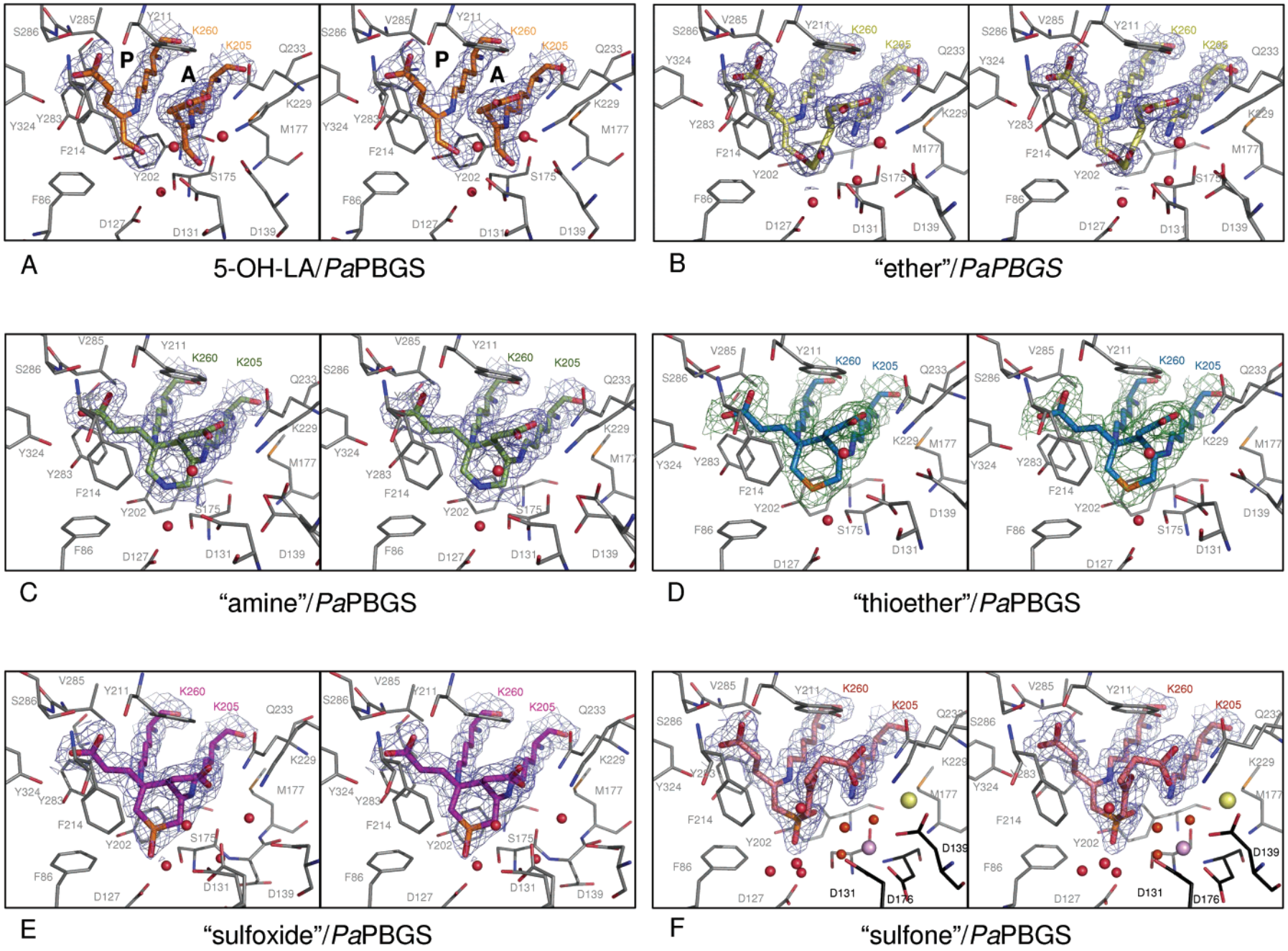
P
A
V285
Y211
K260
K205
Q233
S286
Y324
Y283
K229
M177
F214
Y202
S175
F86
D127
D131
D139
A
5-OH-LA/PaPBGS
B
"ether"/PaPBGS
C
"amine"/PaPBGS
D
"thioether"/PaPBGS
E
"sulfoxide"/PaPBGS
D176
F
"sulfone"/PaPBGS

FIGURE 3: Structures of the six inhibitors bound to *Pa*PBGS with labels according to *Pa*PBGS numbering. All nitrogen, oxygen, and sulfur atoms are colored blue, red, and yellow, respectively, according to the CPK color convention. Carbon atoms of K205 and K260 are colored with the same color as the respective inhibitor carbon atoms. (A) 5-OH-LA (orange) bound to K205 (A-site) and K260 (P-site) through Schiff base linkages. The blue mesh represents the electron density at level of 1.0σ. Surrounding residues are colored gray, and water molecules are depicted as red spheres. (B) "Ether" (yellow) bound to K260 (P-site) via a Schiff base. Clearly no intramolecular bond was formed. The blue mesh represents the electron density at a level of 1.0σ. C3−C5 of the inhibitor molecule are not defined by electron density and are modeled as the most likely conformation due to conformational restraints. Surrounding residues are colored in gray, and water molecules are depicted as red spheres. D139 exhibits two alternative conformations. (C) "Amine" (green) bound to K205 (A-site) and K260 (P-site) via a Schiff base and a single bond, respectively. The blue mesh represents the electron density at a level of 1.0σ. The aldole reaction between C3 and C8 of the inhibitor has created a new bond as shown by the continuous electron density between these two atoms. Surrounding residues are colored gray, and water molecules are depicted as red spheres. D139 exhibits two alternative conformations. (D) "Thioether" (blue) bound to K205 (A-site) and K260 (P-site) via a Schiff base and a single bond, respectively. The green mesh represents the electron density at a level of 1.0σ. The aldole reaction between C3 and C8 of the inhibitor has created a new bond as shown by the continuous electron density between these two atoms. Surrounding residues are colored gray, and water molecules are depicted as red spheres. (E) "Sulfoxide" (purple) bound to K205 (A-site) and K260 (P-site) via a Schiff base and a single bond, respectively. The blue mesh represents the electron density at a level of 1.0σ. The aldole reaction between C3 and C8 of the inhibitor has created a new bond as shown by the continuous electron density between these two atoms. Surrounding residues are colored gray, and water molecules are depicted as red spheres. D131 exhibits two alternative conformations. (F) "Sulfone" (salmon) bound to K260 (P-site) via a Schiff base. Clearly no intramolecular bond was formed. The blue mesh represents the electron density at a level of 1.0σ. Surrounding residues are colored gray, and water molecules are depicted as red spheres. D131 exhibits two alternative conformations. A magnesium ion (light purple) and a chloride ion (light yellow) are bound to the active site.

the polarity. These changes are accompanied by the emergence of a second conformation for residues 136−138 and a disordered active site flap. The remainder of the active site nevertheless is unaffected.

Among the diketo inhibitors, "sulfone" exhibits the most unexpected mode of binding, unmatched by any other PBGS structure so far (Figure 3F). It is covalently fixed only with one of its keto groups via a Schiff base to K260 in the P-site. As in "ether"/*Pa*PBGS, the second Schiff base is not formed, and coincidentally, the conformation of its P-site part resembles the P-sites of 5F-LA/*Pa*PBGS, 5-OH-LA/*Pa*PBGS, and ALA/*Sc*PBGS (Figure 4B). Furthermore, the A-side part of "sulfone" is clearly defined by electron density. The respective carboxylic moiety lies in the expected position but with an orientation tilted by 90° highlighting the degree of structural flexibility in this part of the active center. The formation of the second Schiff base has not yet occurred; instead, the keto group oxygen and one of the sulfonyl oxygen atoms are within H-bonding distance of N_ϵ of K205. This unexpected conformation is very likely a precondition for the binding of a metal ion in the active site, coordinated by D131, D139, D176, and three water molecules (Figures 3F and 4D). Several indications are consistent with the need for a magnesium ion: an octahedral coordination sphere, the distances of 2.02−2.17 Å between the coordinating oxygen atoms and the metal ion (*22* and references cited therein), and the amount of electron density (calcium, manganese, or zinc ions would fit the electron density at only low occupancies). Furthermore, magnesium is the only divalent cation present in significant amounts in the purification and crystallization solutions. The inhibitor chelates the supposed magnesium ion indirectly. Two of the magnesium ion coordinating water molecules are within H-bonding distance of the carboxylic moiety of the A-side part of the inhibitor. The third water molecule is part of a hydrophilic network comprising D127, S175, the sulfonyl moiety of the inhibitor, and another water molecule. Additionally, circular-shaped electron density was found adjacent to the magnesium binding site that could not be sufficiently explained by a water molecule. Instead, it was interpreted as a chloride ion fitting well the electron density. It exhibits a relatively short H-bond to one of the magnesium ion coordinating residues (2.86 Å) as well as two long H-bonds to the backbone amide of M177 (3.22 Å) and the side chain amide nitrogen of Q233 (3.29 Å). This chloride ion completes a network of H-bond donors and acceptors. This is the first time that either a magnesium or a chloride ion has been found in the active site of any PBGS structure.

DISCUSSION

Kinetic Measurements

"Amine", "ether", and "thioether" are relatively good inhibitors compared to other compounds assessed previously (*9*), while 5-OH-LA, "sulfone", and especially "sulfoxide" are weaker inhibitors. Interestingly, the inhibition data obtained for "sulfoxide" and "sulfone" could only be fitted to the dose−response equation if a Hill coefficient (h) was introduced. Different events can account for deviations leading to the introduction of Hill coefficients: nonideal behavior of the inhibitor, cooperativity in the binding process due to the multimeric character of the protein, alteration of the multimeric state of the enzyme, more then one binding site per monomer for the inhibitor, etc. (*17*). At this point, we cannot state the reason for these deviations. One might be the alteration of multimeric states of the protein. In this regard, recent findings describe the existence of freely equilibrating alternate PBGS quaternary isoforms, called morpheeins for mutants of the human PBGS (*7*, *33*, *34*). It has been proposed that the wild-type enzyme exists as an equilibrium of octameric and hexameric forms, the latter of which has been shown to have decreased affinity for the substrate due to the loss of interaction between the active site flap and the carboxyl moieties of the A-side ALA (*34*). If this concept holds true for other wild-type PBGSs, inhibitor binding might alter this equilibrium and therefore account for the observed deviations of the Hill coefficient from 1.0. This might then lead to different binding constants for the inhibitors for the different oligomeric states.

Conformational Differences between PBGSs in the Inhibitor Complex Structures

The conformational differences among the six *Pa*PBGS structures are restricted to the loop connecting D131 with

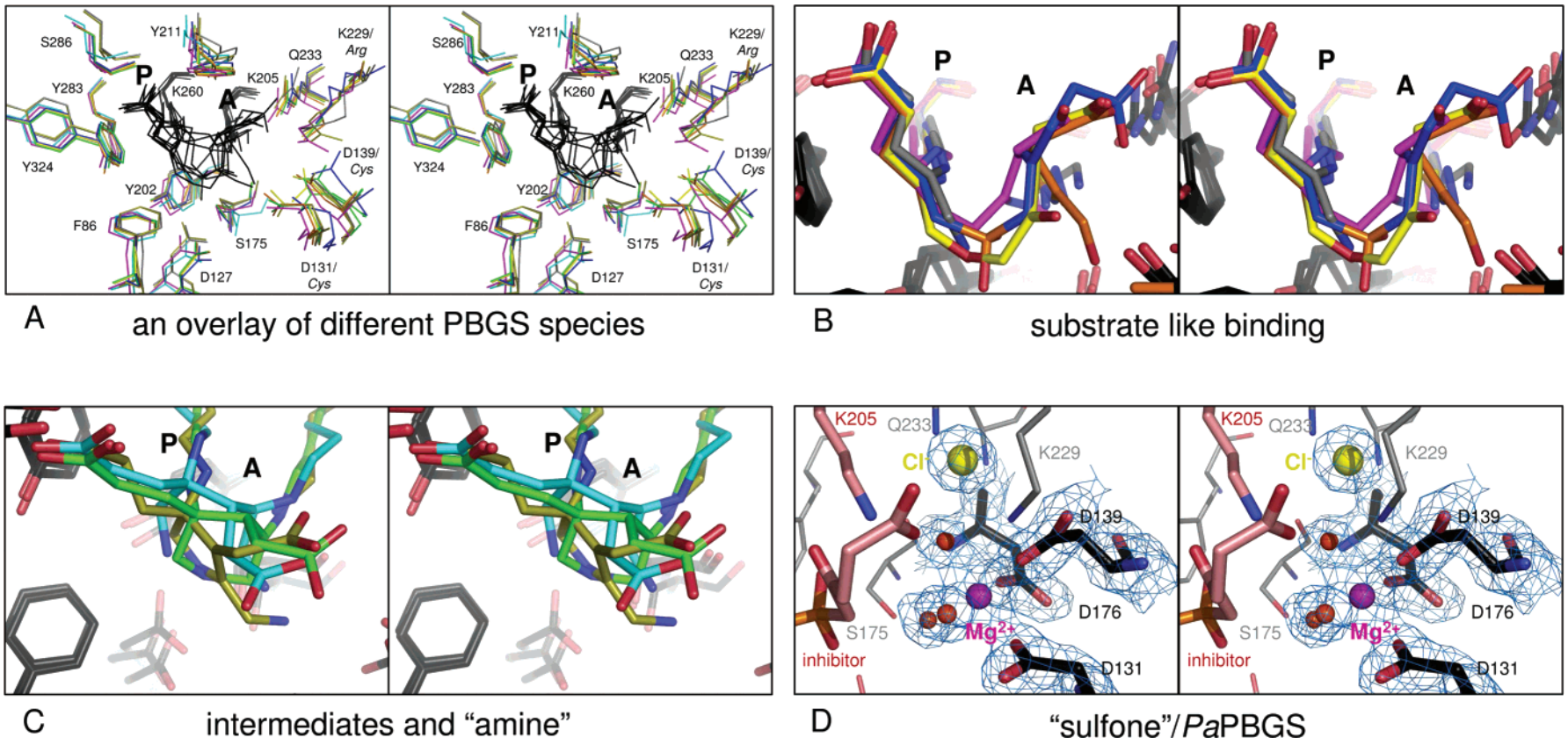

FIGURE 4: Overlays and a close-up of the magnesium binding site in "sulfone"/*Pa*PBGS. (A) Overlay of the residues lining the active centers of 5-OH-LA/*Pa*PBGS (orange), "ether"/*Pa*PBGS (yellow), "amine"/*Pa*PBGS (green), "sulfone"/*Pa*PBGS (blue), ALA/*Sc*PBGS (gray) (*32*), DOSA/*Ec*PBGS (pink) (*28*), intermediate 1/*Hs*PBGS mutant F12L (cyan) (*7*), and intermediate 2/*Sc*PBGS (deep olive) (*13*), with the numbering from *Pa*PBGS, and alternative residues in *Ec*PBGS, *Sc*PBGS, and *Hs*PBGS in italics. The A- and P-site lysines with their bound respective compounds are colored black. Most of the active site residues closely align, while the members of the two flexible loops corresponding to D127, D131, D139, and K229 are less fixed in their positions. Equivalents of D131, D139, and K229 are mutated in the zinc-binding enzymes. In the *Hs*PBGS mutant F12L, equivalents of Q233, D131, D139, and K229 are undetectable due to disordering of this part of the active site in this mutant. When a magnesium ion binds in this region in "sulfone"/*Pa*PBGS, D131 and D139 are significantly shifted compared to those of the other *Pa*PBGS structures. The positioning of the carboxylic group of all compounds in the P-site seems to be very rigid, while there is diversity in the positioning of the second carboxylic group in the A-site. (B) Overlay of 5-OH-LA/*Pa*PBGS (orange), "ether"/*Pa*PBGS (yellow), "sulfone"/*Pa*PBGS (blue), ALA/*Sc*PBGS (gray) (*32*), and DOSA/*Ec*PBGS (purple) (*28*). The conformation of substratelike (unreacted) molecules seems to be structurally conserved in the P-site. The amino moiety of the A-site lysine in DOSA/*Ec*PBGS is forced to the left to accommodate the formation of a second Schiff base; the wounded conformation of DOSA is therefore not suitable for C−C bond formation. (C) Overlay of "amine"/*Pa*PBGS (green), intermediate 1/*Hs*PBGS mutant F12L (cyan) (*7*), and intermediate 2/*Sc*PBGS (deep olive) (*13*). "Amine" is a good mimic of intermediate 1. (D) Magnified view of the magnesium binding site in the active center of "sulfone"/*Pa*PBGS. The electron density at a level of 1.0σ describes the ion and its octahedral coordination sphere formed of D131, D139, D176, and three water molecules that interact with "sulfone" and the chloride ion through H-bonds.

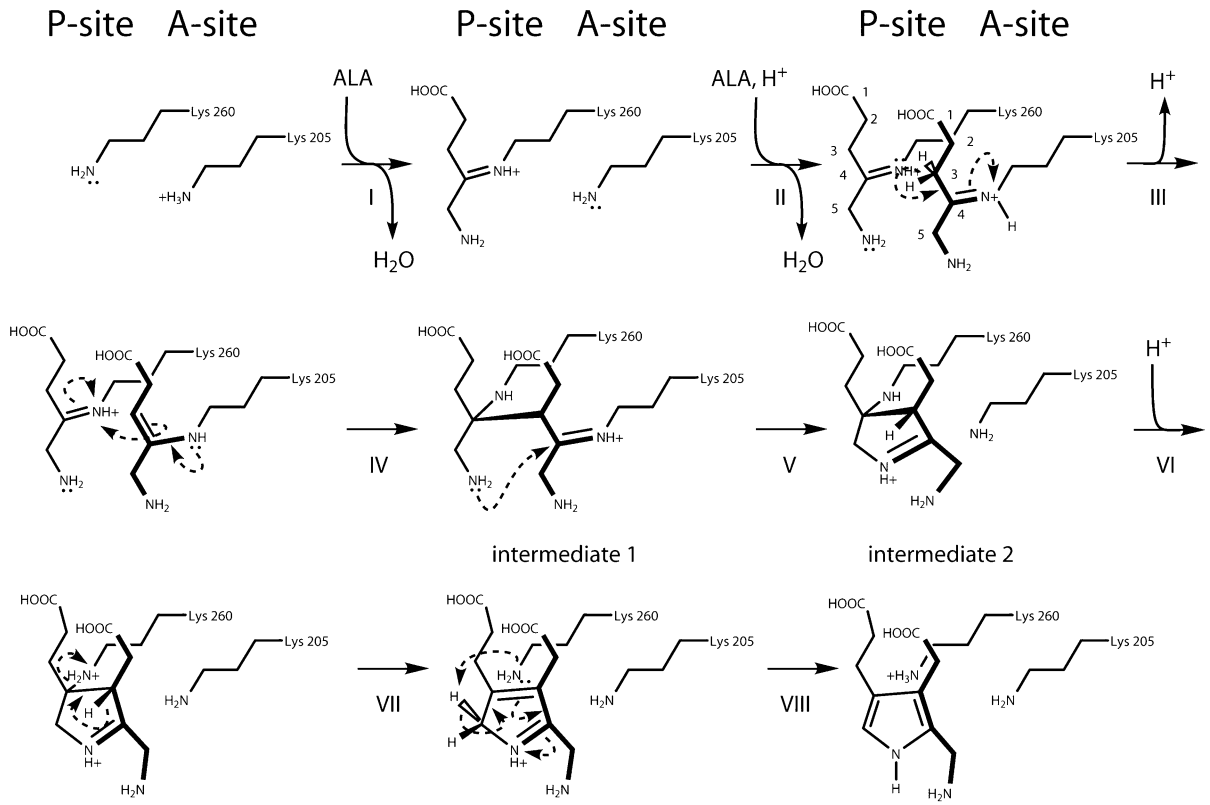

FIGURE 5: Proposed catalytic mechanism of PBGS from *P. aeruginosa*. The steps in the condensation of A- and P-side ALA to form PBG are indicated: (I) binding of P-side ALA, (II) binding of A-side ALA, (III) abstraction of H^+ from C3 of A-side ALA, yielding the A-site enamine, (IV) aldole addition forming the C−C bond between A- and P-side ALA, (V) Schiff base exchange producing a C−N bond between A- and P-side ALA, (VI) transfer of H^+ to Lys260, (VII) trans elimination of P-site lysine, and (VIII) abstraction of the *pro-R* H^+ from C5 of P-side ALA, aromatization, and release of PBG.

D139 and the neighboring active site flap. The remainder of the enzyme and, especially, the rest of the active site appear to be remarkably rigid and unaffected by the binding of different compounds. This observation can be expanded even to structures of PBGSs from other sources with or without different substances bound (Figure 4A). Therefore, the necessary flexibility of the active site is achieved by residues belonging to these two loops. Variations range from the binding of different numbers of water molecules in this region to the presence of a magnesium and chloride ion in the case of "sulfone"/*Pa*PBGS (see below). The flexibility of the loops is also reflected by the temperature factors of the corresponding residues lying well above the average for all structures.

A Magnesium Ion in the Active Site

The binding of a magnesium ion in the active sites of PBGSs lacking the active site zinc binding site has been a continuous matter of discussion. On the basis of kinetic and NMR data, the binding of a magnesium ion in the active site of zinc-free PBGSs had been postulated (*35*, *36*), but so far, all structures of exclusively magnesium binding PBGSs (*5*, *6*, *9*, *10*) showed only a magnesium ion bound to an allosteric binding site distant from the active site. Therefore, the structure of the "sulfone"/*Pa*PBGS complex is the first structural hint that a magnesium ion can truly be stabilized within the active site (Figure 4D). Nevertheless, the interactions stabilizing the magnesium ion in "sulfone"/*Pa*PBGS are partly artificial due to the artificial nature of the bound inhibitor. This finding should therefore not be overrated, but it revives the idea of an intermediary bound magnesium ion participating in catalysis of zinc-free PBGSs.

Catalytic Mechanism of PaPBGS

The comparison of the six different structures of inhibitor/*Pa*PBGS complexes together with recently determined structures now allows us to describe the catalyzed mechanism in more detail.

(I) Binding of P-Site ALA. At first, a stable Schiff base is formed between the substrate molecule's keto moiety and the amino group of the P-site lysine (K260), as proven by several crystal structures and Schiff base trapping studies (Figures 4B and 5, step I) (*4*, *5*, *12*, *15*, *37*−*39*).

(II) Binding of A-Site ALA. In a similar event, the second substrate molecule is bound to the second lysine in the A-site (K205); thereby, the more flexible parts of the active site (D131, D139, R215, and K229) are stabilized by several defined interactions. The active site is shielded from the surrounding medium by the ordering of the active site flap. 5-OH-LA/*Pa*PBGS and 5F-LA/*Pa*PBGS (*9*) resemble this state prior to the onset of catalysis (Figures 3A and 5, step II).

(III) Enamine Formation. In vivo, the second Schiff base formation is transient and followed by the formation of an enamine at the A-site as a prelude to the next step.

(IV) Aldole Addition (formation of the C−C bond). The C−C bond between C3 of the A-site ALA and the P-site ALA is formed by an aldole addition (Figure 5, step IV). The formation of the A-site Schiff base and the enamine as activation seems to be a prerequisite for this reaction step.

This fact is supported by the complexes "ether"/*Pa*PBGS and "sulfone"/*Pa*PBGS (Figure 3B,F), where the second Schiff base is lacking. In these cases, no formation of the C−C bond has occurred which is in contrast to complexes in which the second A-site Schiff base is established ("amine"/*Pa*PBGS, "thioether"/*Pa*PBGS, and "sulfoxide"/*Pa*PBGS). These inhibitor structures thereby support the interpretation of electron density found in the partly disordered active site of *Hs*PBGS that was modeled as this respective intermediate 1 (Figure 5) (*7*). Why does formation of the C−N bond not occur first? Here the comparison among "amine"/*Pa*PBGS, "thioether"/*Pa*PBGS, "sulfoxide"/*Pa*PBGS, and DOSA/*Ec*PBGS (Figure 4B,C) (*14*) helps to explain that formation of the C−C bond can only occur when the compounds possess enough conformational flexibility. This allows the nucleophile (the A-side C3 atom) to attack the electrophile (P-side C4 atom, i.e., C8 atom of the inhibitors) along the Burgi−Dunitz angle. This is most likely the case for the two separate ALA molecules, prior to formation of the C−N bond.

(V) Schiff Base Exchange (formation of the C−N bond). Following the aldole addition, the C−N bond is formed through an attack of the P-side substrate amino moiety on the A-site Schiff base (Figure 5, step V), leading to a Schiff base exchange that sets the A-site lysine free. The intermediate formed this way exactly resembles the intermediate 2/*Sc*PBGS (Figure 4C) and intermediate 2/*Hs*PBGS (*13*, *40*) complexes and was also found in a structure of *Pa*PBGS (unpublished results). The existence of such protein intermediate complexes that are even suitable for crystallization indicates that this state is relatively stable (or metastable). This relative stability might be the explanation for the slow conversion of this intermediate into the product through the lysis of the remaining single bond linking the intermediate to the P-site lysine (Figure 5, step VII). It has been suggested that substrate binding in a neighboring active site of the PBGS multimer triggers a conformational change that facilitates this lysis (*11*). The "amine", "thioether", and "sulfoxide" structures clearly support the assumption of stabilization of closed ring structures by the protein (Figure 3C−E).

(VI) Protonation of P-site lysine and (VII) trans elimination of P-site lysine might thereby be the rate-limiting step of catalysis causing the PBGSs to be slow enzymes with k_{cat} values in the range of 1 s^{-1} and a k_{cat}/K_m of 10 s^{-1} M^{-1}.

(VIII) Abstraction of the pro-R H^+ *from C5 of P-side ALA* (*41*), aromatization, and release of PBG after lysis of the connecting bond between intermediate 2 and the P-site lysine (Figure 5, step VIII) are the last steps of the catalytic process prior to product release.

This last step, the formation of the aromatic ring structure, provides the driving force for the whole reaction.

Why do 5F-LA and 5-OH-LA not form the C−C bond? Obviously, they are not able to form an intermediate with a ring structure that is stabilized by the enzyme, and consequently, the reaction is stalled prior to formation of the C−C bond.

Conclusion and Outlook

The new crystal structures of *Pa*PBGS in complex with several inhibitors presented here allowed us to confirm the catalytic mechanism of *Pa*PBGS proposed in an earlier study (*9*). Comparison with the findings of Erskine et al. (*13*) and Breinig et al. (*7*) and the mechanisms proposed by these groups leads to the conclusion that substrate binding and activation through two Schiff bases, the initial C−C bond formation, and the stabilization of a ring structure intermediate are fundamentals of PBGS catalysis.

Nevertheless, the function of metal ions in the catalytic process remains an open question. The participation of the zinc ion at the active site in zinc-binding enzymes has been postulated (*4*, *11*). The "sulfone"/*Pa*PBGS structure in which a magnesium ion is bound to the active site sheds new light on the direct involvement of magnesium ions in the mechanism for exclusively magnesium binding PBGSs. To tackle this question, new kinetic and crystallization experiments are underway.

ACKNOWLEDGMENT

We are grateful to Linda Stith and Eileen Jaffe for providing pLM_PBGS and for helpful discussion. Thanks are also due to Wolf-Dieter Schubert for help with structure determination. F.F., M.N., and N.F.-D. are grateful to Dieter Jahn for his support.

REFERENCES

1. Jordan, P. M. (1994) Highlights in haem biosynthesis, *Curr. Opin. Struct. Biol. 4*, 902−11.
2. Frankenberg, N., Moser, J., and Jahn, D. (2003) Bacterial heme biosynthesis and its biotechnological application, *Appl. Microbiol. Biotechnol. 63*, 115−27.
3. Erskine, P. T., Senior, N., Awan, S., Lambert, R., Lewis, G., Tickle, I. J., Sarwar, M., Spencer, P., Thomas, P., Warren, M. J., Shoolingin-Jordan, P. M., Wood, S. P., and Cooper, J. B. (1997) X-ray structure of 5-aminolaevulinate dehydratase, a hybrid aldolase, *Nat. Struct. Biol. 4*, 1025−31.
4. Erskine, P. T., Norton, E., Cooper, J. B., Lambert, R., Coker, A., Lewis, G., Spencer, P., Sarwar, M., Wood, S. P., Warren, M. J., and Shoolingin-Jordan, P. M. (1999) X-ray structure of 5-aminolevulinic acid dehydratase from *Escherichia coli* complexed with the inhibitor levulinic acid at 2.0 Å resolution, *Biochemistry 38*, 4266−76.
5. Frankenberg, N., Erskine, P. T., Cooper, J. B., Shoolingin-Jordan, P. M., Jahn, D., and Heinz, D. W. (1999) High-resolution crystal structure of a Mg^{2+}-dependent porphobilinogen synthase, *J. Mol. Biol. 289*, 591−602.
6. Coates, L., Beaven, G., Erskine, P. T., Beale, S. I., Avissar, Y. J., Gill, R., Mohammed, F., Wood, S. P., Shoolingin-Jordan, P., and Cooper, J. B. (2004) The X-ray structure of the plant like 5-aminolaevulinic acid dehydratase from *Chlorobium vibrioforme* complexed with the inhibitor laevulinic acid at 2.6 Å resolution, *J. Mol. Biol. 342*, 563−70.
7. Breinig, S., Kervinen, J., Stith, L., Wasson, A. S., Fairman, R., Wlodawer, A., Zdanov, A., and Jaffe, E. K. (2003) Control of tetrapyrrole biosynthesis by alternate quaternary forms of porphobilinogen synthase, *Nat. Struct. Biol. 10*, 757−63.
8. Bollivar, D. W., Clauson, C., Lighthall, R., Forbes, S., Kokona, B., Fairman, R., Kundrat, L., and Jaffe, E. K. (2004) *Rhodobacter capsulatus* porphobilinogen synthase, a high activity metal ion independent hexamer, *BMC Biochem. 5*, 17.
9. Frere, F., Schubert, W. D., Stauffer, F., Frankenberg, N., Neier, R., Jahn, D., and Heinz, D. W. (2002) Structure of porphobilinogen synthase from *Pseudomonas aeruginosa* in complex with 5-fluorolevulinic acid suggests a double Schiff base mechanism, *J. Mol. Biol. 320*, 237−47.
10. Frere, F., Reents, H., Schubert, W. D., Heinz, D. W., and Jahn, D. (2005) Tracking the evolution of porphobilinogen synthase metal dependence in vitro, *J. Mol. Biol. 345*, 1059−70.
11. Jaffe, E. K. (2004) The porphobilinogen synthase catalyzed reaction mechanism, *Bioorg. Chem. 32*, 316−25.

12. Jaffe, E. K., and Hanes, D. (1986) Dissection of the early steps in the porphobilinogen synthase catalyzed reaction. Requirements for Schiff's base formation, *J. Biol. Chem. 261*, 9348−53.
13. Erskine, P. T., Coates, L., Butler, D., Youell, J. H., Brindley, A. A., Wood, S. P., Warren, M. J., Shoolingin-Jordan, P. M., and Cooper, J. B. (2003) X-ray structure of a putative reaction intermediate of 5-aminolaevulinic acid dehydratase, *Biochem. J. 373*, 733−8.
14. Kervinen, J., Jaffe, E. K., Stauffer, F., Neier, R., Wlodawer, A., and Zdanov, A. (2001) Mechanistic basis for suicide inactivation of porphobilinogen synthase by 4,7-dioxosebacic acid, an inhibitor that shows dramatic species selectivity, *Biochemistry 40*, 8227−36.
15. Erskine, P. T., Coates, L., Newbold, R., Brindley, A. A., Stauffer, F., Wood, S. P., Warren, M. J., Cooper, J. B., Shoolingin-Jordan, P. M., and Neier, R. (2001) The X-ray structure of yeast 5-aminolaevulinic acid dehydratase complexed with two diacid inhibitors, *FEBS Lett. 503*, 196−200.
16. Frankenberg, N., Heinz, D. W., and Jahn, D. (1999) Production, purification, and characterization of a Mg^{2+}-responsive porphobilinogen synthase from *Pseudomonas aeruginosa*, *Biochemistry 38*, 13968−75.
17. Copeland, R. A. (2005) Evaluation of enzyme inhibitors in drug discovery. A guide for medicinal chemists and pharmacologists, *Methods Biochem. Anal. 46*, 1−265.
18. Collaborative Computational Project Number 4 (1994) The CCP4 suite: Programs for protein crystallography, *Acta Crystallogr. D50*, 760−3.
19. Murshudov, G. N., Vagin, A. A., and Dodson, E. J. (1997) Refinement of Macromolecular Structures by the Maximum-Likelihood Method, *Acta Crystallogr. D53* (Part 3), 240−55.
20. Perrakis, A., Morris, R., and Lamzin, V. S. (1999) Automated protein model building combined with iterative structure refinement, *Nat. Struct. Biol. 6*, 458−63.
21. Jones, T. A., Zou, J.-Y., Cowan, S. W., and Kjeldgaard, M. (1991) Improved methods for building protein models in electron density maps and the location of errors in these models, *Acta Crystallogr. A47*, 110−9.
22. Harding, M. M. (2001) Geometry of metal−ligand interactions in proteins, *Acta Crystallogr. D57*, 401−11.
23. Laskowski, R. A., MacArthur, M. W., Moss, D. S., and Thornton, J. M. (1993) PROCHECK: A program to check the stereochemical quality of protein structures, *J. Appl. Crystallogr. 26* (Part 2), 283−91.
24. Hooft, R. W., Vriend, G., Sander, C., and Abola, E. E. (1996) Errors in protein structures, *Nature 381*, 272.
25. Wallace, A. C., Laskowski, R. A., and Thornton, J. M. (1995) LIGPLOT: A program to generate schematic diagrams of protein−ligand interactions, *Protein Eng. 8*, 127−34.
26. Gacond, S. (2005) Ph.D. Thesis, Institut de Chimie, Université de Neuchâtel, Neuchâtel, Switzerland.
27. Jarret, C., Stauffer, F., Henz, M. E., Marty, M., Luond, R. M., Bobalova, J., Schurmann, P., and Neier, R. (2000) Inhibition of *Escherichia coli* porphobilinogen synthase using analogs of postulated intermediates, *Chem. Biol. 7*, 185−96.
28. Stauffer, F., Zizzari, E., Engeloch-Jarret, C., Faurite, J. P., Bobalova, J., and Neier, R. (2001) Inhibition studies of porphobilinogen synthase from *Escherichia coli* differentiating between the two recognition sites, *ChemBioChem 2*, 343−54.
29. Lüönd, R. M., Walker, J., and Neier, R. (1992) Assessment of the active-site requirements of 5-aminolevulinic acid dehydratase: Evaluation of substrate and product analogs as competitive inhibitors, *J. Org. Chem. 57*, 5005−13.
30. Cheung, K. M., Spencer, P., Timko, M. P., and Shoolingin-Jordan, P. M. (1997) Characterization of a recombinant pea 5-aminolevulinic acid dehydratase and comparative inhibition studies with the *Escherichia coli* dehydratase, *Biochemistry 36*, 1148−56.
31. Erskine, P. T., Coates, L., Newbold, R., Brindley, A. A., Stauffer, F., Beaven, G. D. E., Gill, R., Coker, A., Wood, S. P., Warren, M. J., Shoolingin-Jordan, P. M., Neier, R., and Cooper, J. B. (2005) Structure of yeast 5-aminolaevulinic acid dehydratase complexed with the inhibitor 5-hydroxylaevulinic acid, *Acta Crystallogr. D61*, 1222−6.
32. Erskine, P. T., Newbold, R., Brindley, A. A., Wood, S. P., Shoolingin-Jordan, P. M., Warren, M. J., and Cooper, J. B. (2001) The X-ray structure of yeast 5-aminolaevulinic acid dehydratase complexed with substrate and three inhibitors, *J. Mol. Biol. 312*, 133−41.
33. Jaffe, E. K. (2005) Morpheeins: A new structural paradigm for allosteric regulation, *Trends Biochem. Sci. 30*, 490−7.
34. Tang, L., Breinig, S., Stith, L., Mischel, A., Tannir, J., Kokona, B., Fairman, R., and Jaffe, E. K. (2006) Single amino acid mutations alter the distribution of human porphobilinogen synthase quaternary structure isoforms (morpheeins), *J. Biol. Chem. 281*, 6682−90.
35. Petrovich, R. M., and Jaffe, E. K. (1997) Magnetic resonance studies on the active site and metal centers of *Bradyrhizobium japonicum* porphobilinogen synthase, *Biochemistry 36*, 13421−7.
36. Petrovich, R. M., Litwin, S., and Jaffe, E. K. (1996) *Bradyrhizobium japonicum* porphobilinogen synthase uses two Mg(II) and monovalent cations, *J. Biol. Chem. 271*, 8692−9.
37. Gibbs, P. N., and Jordan, P. M. (1986) Identification of lysine at the active site of human 5-aminolaevulinate dehydratase, *Biochem. J. 236*, 447−51.
38. Spencer, P., and Jordan, P. M. (1995) Characterization of the two 5-aminolaevulinic acid binding sites, the A- and P-sites, of 5-aminolaevulinic acid dehydratase from *Escherichia coli*, *Biochem. J. 305* (Part 1), 151−8.
39. Erskine, P. T., Newbold, R., Roper, J., Coker, A., Warren, M. J., Shoolingin-Jordan, P. M., Wood, S. P., and Cooper, J. B. (1999) The Schiff base complex of yeast 5-aminolaevulinic acid dehydratase with laevulinic acid, *Protein Sci. 8*, 1250−6.
40. Mills-Davies, N. L., Thompson, D., Cooper, J. B., Wood, S. P., and Shoolingin-Jordan, P. M. (2000) RCSB Protein Data Bank, PDB Code 1E51.
41. Chaudhry, A. G., and Jordan, P. M. (1976) Stereochemical studies on the formation of porphobilinogen, *Biochem. Soc. Trans. 4*, 760−1.
42. Brünger, A. T. (1992) Free *R*-value: A novel statistical quantity for assessing the accuracy of crystal structures, *Nature 355*, 472−5.